# Oxygen crystallographic positions in thin films by non-destructive resonant elastic X-ray scattering

Antonio Peña Corredor, Laurianne Wendling, Daniele Preziosi, Laurent Schlur, Cédric Leuvrey, Dominique Thiaudière, Erik Elklaim, Nils Blanc, Stephane Grenier, François Roulland, et al.

JOURNAL OF APPLIED CRYSTALLOGRAPHY

ISSN 1600-5767

# Oxygen crystallographic positions in thin films by non-destructive resonant elastic X-ray scattering

**Antonio Peña Corredor,[a]* Laurianne Wendling,[a] Daniele Preziosi,[a] Laurent Schlur,[a] Cédric Leuvrey,[a] Dominique Thiaudière,[b] Erik Elklaim,[b] Nils Blanc,[c] Stephane Grenier,[d] François Roulland,[a] Nathalie Viart[a] and Christophe Lefevre[a]**

[a]DCMI, Institut de Physique et Chimie des Matériaux de Strasbourg, 23 rue du Loess, Strasbourg, 67200, France, [b]Synchrotron SOLEIL, L'Orme des Merisiers Saint-Aubin BP 48, Gif-sur-Yvette, 91192, France, [c]European Synchrotron Radiation Facility, 71 avenue des Martyrs, Grenoble, 38043, France, and [d]Institut Néel, 25 rue des Martyrs BP 166, Grenoble, 38042, France. *Correspondence e-mail: antonio.penacorredor@ipcms.unistra.fr

Received 27 October 2021
Accepted 2 April 2022

Edited by A. Borbély, Ecole National Supérieure des Mines, Saint-Etienne, France

**Keywords:** resonant elastic X-ray scattering; REXS; extended diffraction absorption fine structure; EDAFS; non-destructive characterization; oxygen positions; thin films.

**Supporting information**: this article has supporting information at journals.iucr.org/j

Precisely locating oxygen atoms in nanosized systems is a real challenge. The traditional strategies used for bulk samples fail at probing samples with much less matter. Resonant elastic X-ray scattering (REXS) experiments in the X-ray absorption near-edge structure (XANES) domain have already proved their efficiency in probing transition metal cations in thin films, but it is not feasible to perform such experiments at the low-energy edges of lighter atoms – such as oxygen. In this study, the adequacy of using REXS in the extended X-ray absorption fine structure (EXAFS) domain, also known as extended diffraction absorption fine structure (EDAFS), to solve this issue is shown. The technique has been validated on a bulk $FeV_2O_4$ sample, through comparison with results obtained with conventional X-ray diffraction measurements. Subsequently, the positions of oxygen atoms in a thin film were unveiled by using the same strategy. The approach described in this study can henceforth be applied to solve the crystallographic structure of oxides, and will help in better understanding the properties and functionalities which are dictated by the positions of the oxygen atoms in functional nanosized materials.

## 1. Introduction

Oxide thin films are a topic of increasing research relevance owing to their potential applications in conventional electronics, spintronics and orbitronics (Bibes *et al.*, 2011; Trier *et al.*, 2021; Vaz *et al.*, 2018). The properties of these films are very sensitive to their crystallographic structure. As a result, there is particular interest in determining the positions of the atoms present in the crystal (Tan *et al.*, 2019).

In oxide materials, knowing where the oxygen atoms are is crucial to fully picture the crystal structure of the sample. Oxygen atoms can also play a major role in the properties of functional oxides. Locating them is thus necessary to explain the phenomena behind such properties and is a preliminary step before the use of oxide materials in functional devices. One example is magnetically active or ferroelectric oxides, where knowledge of the oxygen positions is needed to explain the arrangement responsible for the material's behavior (Giovannetti *et al.*, 2011; Zhou *et al.*, 2019). Equally, in oxides with orbitally ordered states, locating the oxygen atoms allows one to understand the structural deformations which lead to the orbital order inside the material (Kawaguchi *et al.*, 2016).

For bulk materials, synchrotron X-ray diffraction (S-XRD) and neutron diffraction (ND) techniques are commonly used

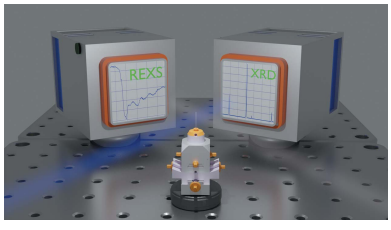

to locate the different atoms that compose the crystal (Woińska *et al.*, 2016; Shahzad *et al.*, 2011; Blum *et al.*, 2009). However, these methods have difficulties in giving a whole picture of the crystal structure of thin-film samples. Thin films have much less matter to probe, limiting a potential crystallographic unveiling via ND. Furthermore, they possess a strong preferred crystal orientation, which hinders a complete crystallographic study through conventional S-XRD.

A possibility for such systems is precession electron diffraction, a technique coupled with transmission electron microscopy which allows solving the structure of thin-film materials (Steciuk *et al.*, 2019; Rotella *et al.*, 2015). Despite its potency in obtaining accurate structure models, this technique requires a tedious and destructive sample preparation process. Therefore, a friendlier approach for the crystallographic unveiling of thin films is desirable.

An alternative for the presented issues would be resonant elastic X-ray scattering (REXS) in the X-ray absorption near-edge structure (XANES) domain, also known as diffraction anomalous near-edge structure (DANES). Differently from conventional diffraction techniques, DANES experiments consist of an energy scan around the absorption edge of one of the present atoms, for a fixed reflection position of the reciprocal lattice. This approach is based on the fact that the dispersive terms [$f'(E)$ and $f''(E)$] of the atomic scattering factor [$f(Q, E) = f_0(Q) + f'(E) + if''(E)$] are energy dependent.

DANES has already been shown to be successful in probing the metallic cations in oxide thin films through resonance at their $K$ edges (Lefevre *et al.*, 2017; Thomasson *et al.*, 2013). Resonance at the absorption edge of oxygen is, however, not feasible in practice, owing to the low energy (530 eV) (Frati *et al.*, 2020) and hence long wavelength (2.3 nm) of this edge. These values imply that the absorption is too strong (Tröger *et al.*, 1992) and the impossibility of studying small-sized crystallographic cells, such as those of most oxides. As a result, the direct probing of oxygen atoms is not straightforward.

In the XANES region, around the cation absorption edge, the information predominantly originates from the cation (its oxidation state, occupation factor . . . ). Owing to its predominant influence in this domain, it is hard to extract information about the surrounding ligands. Fortunately, the extended X-ray absorption fine structure (EXAFS) domain, which starts at around +50 eV above the cation absorption edge, does contain such information (Favre-Nicolin, 1999). We therefore propose the exploration of a wide energy range, just below and covering a substantial range above the absorption edge, for an accurate determination of the position of the oxygen atoms.

REXS in the EXAFS domain (also known as extended diffraction absorption fine structure, EDAFS) has already been used to solve crystallographic structures by the analysis of the EXAFS oscillations, which can be related to the interatomic distances (Stragier *et al.*, 1992; Katcho *et al.*, 2009). Scanning beyond a cation's edge, one can place its surrounding ligands in a sphere whose radius is the interatomic distance. If the ligands are in a position ($x$, $y$, $z$) that depends on several parameters, more than one solution will place them in the described sphere, and it will be hard to unequivocally locate them by this approach.

In this study, we propose to directly fit the EDAFS spectra for the refinement of the oxygen positions. For this, the structure factor on the EXAFS part is simulated, and then the intensity of the whole fine structure is compared with the measured value. This approach has already been used to characterize structural distortions and other phenomena that only concerned the cation itself (Joly *et al.*, 2008). Our aim is to show that one can also unambiguously locate the surrounding oxygen atoms by indirectly probing around the cation's EXAFS.

The methodology for the validation has been, in the first place, to theoretically demonstrate that EDAFS spectra are indeed sensitive to the oxygen-atom positions. Prior to the experimental validation, we have proven that it is feasible to unequivocally determine these positions through a fitting procedure of REXS spectral intensities with the *FDMNES* software (Bunău & Joly, 2009).

Secondly, the whole procedure has been experimentally validated. The spinel iron vanadate, $FeV_2O_4$ (FVO), has been chosen as a showcase material. At room temperature and in the bulk form, FVO crystallizes in the $Fd\bar{3}m$ (227) space group. $V^{3+}$ and $Fe^{2+}$ cations occupy the 16$d$ and 8$a$ fixed special positions, respectively, whereas oxygen occupies the 32$e$ special position ($x$, $x$, $x$), which depends on the $x$ parameter (Zhang *et al.*, 2012). As a result, the fitting of the atomic positions only involves one single parameter ($x$). At low temperatures or in the form of thin films, the structure becomes tetragonal ($I4_1/amd$) and the oxygen position (16$h$) depends on two parameters (0, $y$, $z$).

In terms of properties, the material has been shown to present ferrimagnetism (MacDougall *et al.*, 2012), ferroelectricity (Zhao *et al.*, 2015) (and hence a multiferroic behavior; Eremin, 2019), an orbital-ordered state (Xie *et al.*, 2019), a possible spin-glass-like behavior (Nishihara *et al.*, 2010) and a potential use in Na-ion batteries (Maggay *et al.*, 2018) among other functionalities. Most of these properties are strongly impacted by the positions of the oxygen atoms. This is why their determination is so crucial, and this is what makes FVO a perfect candidate for the validation of the proposed method.

EDAFS measurements have been carried out on a bulk FVO sample and, by fitting the spectra with *FDMNES*, a value for the oxygen position has been found. Conventional S-XRD measurements have been performed on the same bulk sample and lead to the same value for the oxygen position. We have thus shown that information on the position of the oxygen atoms can be successfully extracted from the fitting of an experimental EDAFS spectrum. Finally, we have applied the whole method on a thin film of FVO, in order to determine the position of the oxygen atoms in a system in which the quantity of matter is small.

As a result, this study constitutes a proof of the efficiency of EDAFS to indirectly probe oxygen atoms by fitting the experimental spectra around the cation's EXAFS and its adequacy to nondestructively analyze nanosized systems, where most conventional diffraction studies fail to achieve the goal that we pursue.

## 2. Experimental

To elaborate FVO powder, a stoichiometric mixture of $Fe_2O_3$ (Sigma–Aldrich, 99.6%) and $V_2O_5$ (STREM CHEMICALS, 99.8%) was manually ground in an agate mortar for 15 min, with a small quantity of ethanol. The resulting powder was first heated to 873 K for 10 h in a reducing atmosphere of $H_2$/Ar (2.5:97.5) to reduce $V_2O_5$ and $Fe_2O_3$ from their V(V) and Fe(III) to their V(III) and Fe(II) states, respectively. Secondly, a calcination was performed at 1373 K for 10 h, using the same reducing atmosphere, to form the desired spinel phase. The resulting calcinated powder was milled through attrition using 0.8 mm-diameter ZrO balls in ethanol for 2 h. The grain size, measured using a granulometer, was of the order of 1 µm.

Finally, the fine powder was uniaxially pressed in the form of a cylindrical pellet and sintered at 1573 K for 20 h, using the same reducing atmosphere as for the calcination. The stoichiometry of the synthesized compound was checked using energy-dispersive X-ray spectroscopy. A V:Fe ratio of 1.97 ± 0.07 was measured, close to the expected value of 2.0.

The FVO pellet was then used to grow 25 nm-thick FVO(001) films onto MgO(001) single crystals (lattice mismatch: 0.4%) by pulsed laser deposition. The pellet was ablated by a KrF excimer laser (λ = 248 nm) with a fluence of 3 J cm$^{-2}$ and a repetition rate of 5 Hz. The deposition took place in a $10^{-2}$ mbar (= 1 Pa) partial pressure, keeping the substrate at a temperature of 673 K. These conditions are based on a previous optimization of stoichiometric MgO// FVO thin films by our team (Roulland *et al.*, 2022).

The bulk sample was ground and inserted into a capillary powder. REXS measurements were carried out at the DIFFABS beamline of the SOLEIL Synchrotron, covering an energy range of (−40 eV, +240 eV) around the Fe *K* edge (around 7130 eV) (Husain *et al.*, 2018), widely scanning thus both XANES and EXAFS parts of the Fe absorption spectrum. A dedicated Python code was developed for the treatment and refinement of these EDAFS data. S-XRD measurements with λ = 0.67122 nm were performed at the CRISTAL beamline. The refinement of the S-XRD data was carried out using the *FullProf–WinPLOTR* software (Roisnel & Rodríquez-Carvajal, 2001), and the oxygen positions were fitted using the Rietveld method (Rietveld, 1969). For the thin film, REXS experiments were performed at the D2AM beamline of the ESRF synchrotron with the same energy range as the powder sample. All measurements took place at room temperature.

## 3. Simulation

REXS spectra were simulated using *FDMNES* (Bunău & Joly, 2009). This software uses time-dependent differential functional theory with the Hubbard correction (LDA+U) for spectrum generation. The Green function formalism was used. The complete set of parameters used in the simulations is described in the supporting information S1.

All the parameters, including the lattice parameter and the positions of the cations, were fixed except for the oxygen-atoms positions ($x$). For this simulation part, structure parameters were taken from the literature (Kawaguchi *et al.*, 2016). For reasons of geometry, $x$ is expected to have a value close to 0.25, and spectra were therefore simulated in the range $x$:[0.230–0.280]. Theoretical spectra (TS) for V and Fe ions were treated independently.

In actual experiments, the acquisition of EDAFS spectra at all reciprocal lattice points (RLPs) would not be practical, so a choice of RLP must be preliminarily made depending on their adequacy. Two parameters have been considered for the evaluation of RLPs: their intensity ($I$) and their sensitivity ($S$) to the oxygen positions, as defined in equation (1):

$$S = \int_{x_{\min}}^{x_{\max}} \int_{E_{\min}}^{E_{\max}} \left[ I_{\mathrm{TS}(x)}(E) - I_{\mathrm{av}}(E) \right]^2 \mathrm{d}E\, \mathrm{d}x. \qquad (1)$$

The sensitivity calculation for a specific RLP compares the simulated intensity for a specific $x$ and at a specific energy $E$, $I_{\mathrm{TS}(x)}(E)$, with the average simulated intensity at this specific energy, for all the considered $x$ values, $I_{\mathrm{av}}(E)$. All the active RLPs of FVO can be positioned in an $I$ versus $S$ plot, as represented in Fig. 1.

A weight factor can be defined considering both parameters: $W_j = S_j I_j$. In the case of the V (Fe) edge, after normalization of the weight factors ($\sum_j W_j = 1$, on all $i$ reflections), two RLPs account for 63% (70%) of the weight sum: 044 – 35% (36%), the most intense; 333 – 28% (34%), the most sensitive. Consequently, among all actively diffracting RLPs, only these two reflections will be considered for the acquisition of experimental data.

In terms of the edge choice, oxygen atoms at $(x, x, x)$ are directly connected to the two cations (Fe, V), so both are equally valid for the purpose of this study. As shown in Fig. 2, for the two RLPs which are being considered, the relative sensitivity and intensity are similar at both absorption edges. The main difference appears in their energy: 5481 eV for V (Frank *et al.*, 1998) and 7111 eV for Fe (Husain *et al.*, 2018; Alderman *et al.*, 2017). Owing to the smaller wavelength of the incident X-rays, this latter edge will present fewer self-absorption issues and a better signal-to-noise ratio, allowing a more exact determination of the oxygen positions. Therefore, EXAFS spectra have been studied around the Fe absorption edge.

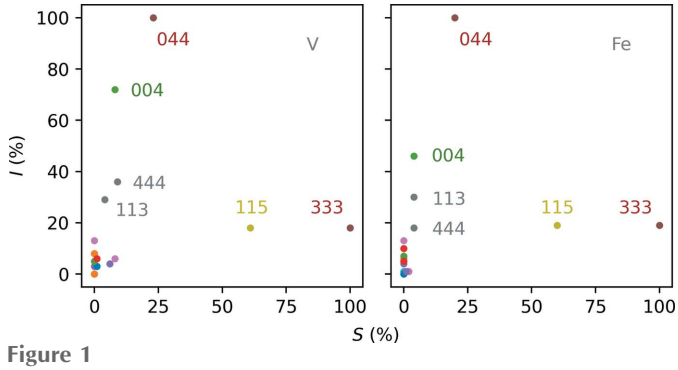


**Figure 1**
Intensity versus sensitivity to the oxygen position for all actively diffracting RLPs for FVO, for both the V and Fe *K* edges.

To prove whether it is possible to fit EXAFS spectra and obtain the oxygen positions, a first fitting process was performed on a pseudo-experimental spectrum (p-ES). For that purpose, a Gauss-centered random noise was added to the simulated theoretical spectra, as shown in the supporting information S2.

At a later stage, a random Gauss-centered energy shift was introduced, simulating the experimental conditions encountered in REXS measurements. The whole process of noise addition and energy shift displacement has been described in the supporting information S2.

The noise generation and fitting processes were repeated 10 000 times, allowing the estimation of an error bar through the bootstrap method. The calculation of this error has also been described in the supporting information S2.

The resulting p-ES, generated with $x = 0.25$ and zero energy shift, was then fitted by comparison with the theoretical spectra. For each $x$ and energy shift ($E_i$) value, a difference ($X^2$) between the intensity of p-ES, $I_{\text{p-ES}}(E)$, and the TS, $I_{\text{TS}(x=x_i)}(E + E_i)$, is calculated, as defined in equation (2):

$$X^2_{j\,(x_i,E_i)} = \int_{E_{\min}}^{E_{\max}} \left[ I_{\text{p-ES}}(E) - I_{\text{TS}(x=x_i)}(E + E_i) \right]^2 \mathrm{d}E. \qquad (2)$$

This process is repeated for all considered reflections ($j$).

When considering the whole set of reflections that are studied, the total error takes the form shown in equation (3):

$$X^2_{(x_i,E_i)} = \sum_j X^2_{j(x_i,E_i)}. \qquad (3)$$

The fitting of the Fe edge p-ES leads to a minimum $x$ = 0.2500 (2), as displayed in Fig. 3, close to the expected initial value (0.25).

The determination of the position of the oxygen atoms through fitting of the EDAFS spectra is therefore theoretically feasible.

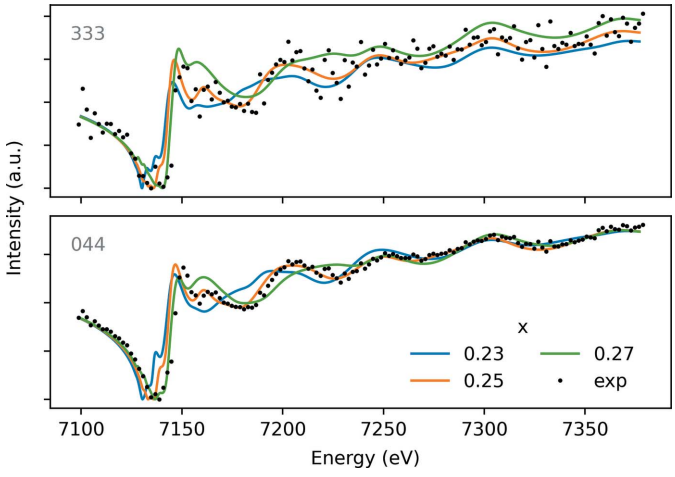


**Figure 2**
p-ES for $x = 0.25$ (black) and TS (colored) for various $x$ values, around the Fe $K$ edge for the 333 and 044 reflections.

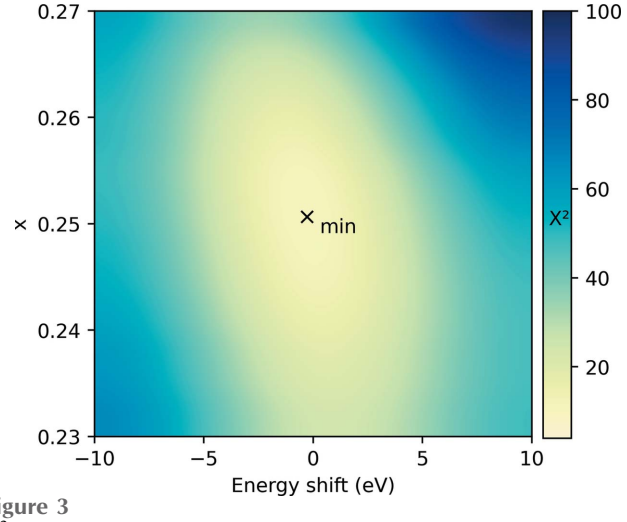


**Figure 3**
$X^2$ as a function of the oxygen position, $x$, and the energy shift. The cross labeled 'min' represents the $x$ and energy shift coordinates leading to the smallest $X^2$.

## 4. Experimental results

The S-XRD diffractogram measured for the synthesized FVO powder is shown in Fig. 4. The representation and fitting of the diffractogram was carried out with *Fullprof*. A negligibly small parasite phase belonging to the $Fe_2O_3$ precursor can be observed, but, since the refinement is based on the position and relative intensities of FVO peaks, it does not interfere with the results of our study.

The lattice constant was calculated by a profile matching analysis: $a$ = 0.845750 (7) nm, consistent with previously reported results (Kawaguchi *et al.*, 2016). Using this value, a Rietveld refinement was carried out, leading to $x$ = 0.262 (2) for the oxygen-atom positions. The complete set of refined atomic positions is listed in Table 1.

REXS spectra were acquired on the same capillary as the S-XRD data. The Fe absorption edge was chosen on the 333 and 044 reflections, because they showed better reliability in the simulation part of this study. Owing to the powdered nature of the sample, when measuring the 333 reflection, the

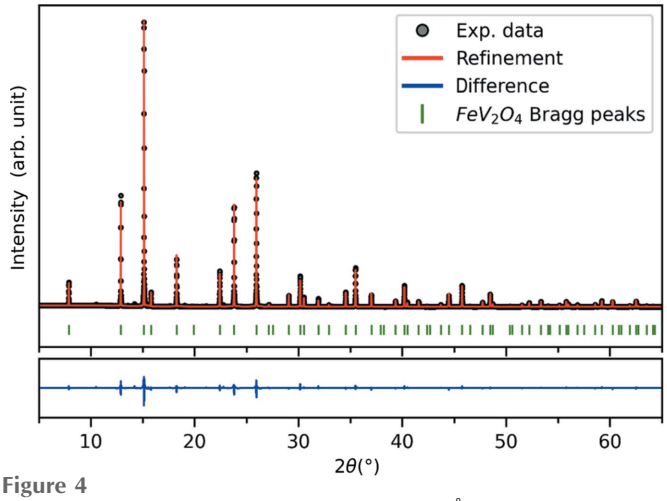


**Figure 4**
S-XRD experimental diagram for λ = 0.67122 Å (black) and the best refinement obtained with *Fullprof* (red).

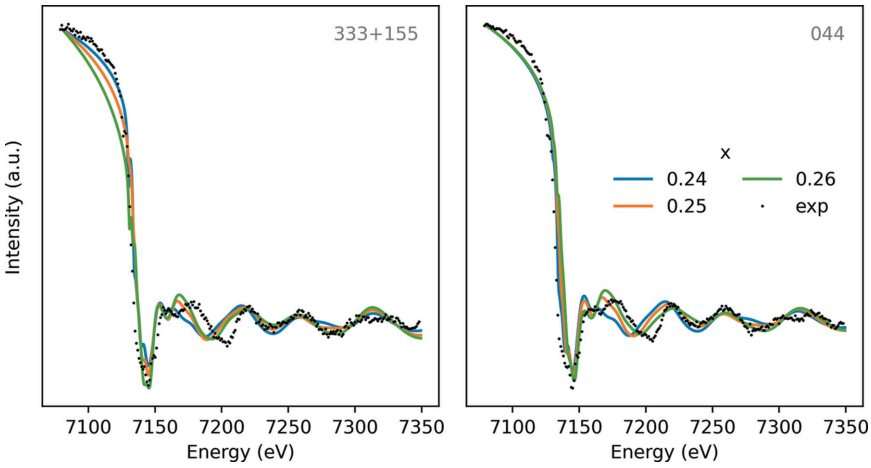


**Figure 5**
REXS spectra acquired at the Fe edge for the 333 and 044 reflections, compared with the simulated TS at different $x$.

acquired intensity would also include the 511 reflection (for both, $h^2 + k^2 + l^2 = 27$). As a result, we considered a combined 333 + 511 reflection with a relative weight of 54%, as defined in Section 3. The two chosen reflections, 044 and 333/511, would thus account for a total of 80% of the weight sum.

*FDMNES* was again used to simulate spectra for a complete meshing of oxygen positions and energy shifts. The powder sample presented a considerable self-absorption, which was also taken into account in our simulations. Ideal occupancy factors (Fe: 8/192; V: 16/192; O: 32/192) were considered. A fitting of these factors shows that the experimental occupancy factors coincide with the ideal values.

The experimental REXS spectra are compared with the simulated ones in Fig. 5. Slope and intensity normalization corrections, depending not on the material itself but on the measurement conditions, were performed before data analysis.

The same procedure applied on the p-ES was repeated on the experimental spectra. The results of the refinement procedure can be seen in Fig. 6, with $x = 0.2625$ (2). This value found for the oxygen positions perfectly matches the one obtained via the Rietveld refinement of the S-XRD data. The procedure was repeated varying by ±20 eV the starting energy value for the refinement (7200 eV). This led to negligible changes in the oxygen-position value and the energy shifts.

Another refinement using the already described procedure was the XANES part of the Fe absorption spectrum (7050–7200 eV). Oppositely to EDAFS fitting, the refinement conditions highly affected the found value for the oxygen positions. In addition, the error was too high to consider the results reliable. Scanning the EXAFS part of the spectrum, which mostly depends on the oxygen atoms (neighboring ligands), hence seems necessary for an exact determination of their positions.

The whole EDAFS procedure was then applied to a 25 nm MgO//FVO thin-film sample. Owing to the substrate strain, FVO presents a distorted spinel tetragonal structure, crystallizing in the $I4_1/amd$ space group. As a result, the oxygen-atom positions in the thin film $(0, y, z)$ depend on two parameters. Analogously to what was done for the bulk sample, in the $X^2$ minimization the energy shift was considered as a third parameter, minimizing it for each $(y, z)$ set.

MgO crystallizes in the $Fm3m$ space group ($a = 0.421$ nm) and has 022 as an active reflection. Since the substrate comprises much more matter than the thin film, it completely eclipses the 044 reflection of FVO, which becomes unexploitable. The chosen RLPs are then 311 and 511.

The lattice parameters of the FVO film are $c$ = 0.8.441 (7) nm and $a = b = 0.8463$ (3) nm. The complete structural characterization of the film is detailed in the supporting information S3. This structural information has been used for the generation of the theoretical spectra. The $X^2$ minimum was found for $y = 0.467$ (1) and $z = 0.267$ (1), as shown in Fig. 7. These values fit the 311 and 511 spectra well, as shown in Fig. 8. The complete set of atomic positions for the thin film is listed in Table 2.

The signal-to-noise ratio is not as good as for the bulk, but it has been possible to find a mathematical minimum and thus locate the oxygen atoms. The scanning of additional RLPs

**Table 1**
Atomic positions of bulk FVO ($Fd\bar{3}m$ group, origin choice 2).

| Atom | Position | Atomic coordinates |
|---|---|---|
| Iron | 8*a* | 0.125, 0.125, 0.125 |
| Vanadium | 16*d* | 0.5, 0.5, 0.5 |
| Oxygen | 32*e* | 0.262 (2), 0.262 (2), 0.262 (2) |

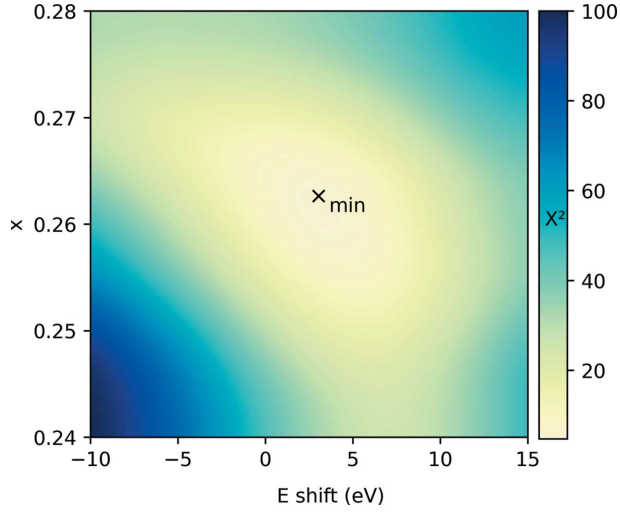


**Figure 6**
$X^2$ as a function of $x$ (oxygen position) and the energy shift, for the experimental spectra.

Table 2
Atomic positions of FVO thin films ($I4_1/amd$ group, origin choice 2).

| Atom | Position | Atomic coordinates |
|---|---|---|
| Iron | 4*a* | 0, 0.75, 0.125 |
| Vanadium | 8*d* | 0, 0, 0.5 |
| Oxygen | 16*h* | 0, 0.467 (1), 0.267 (1) |

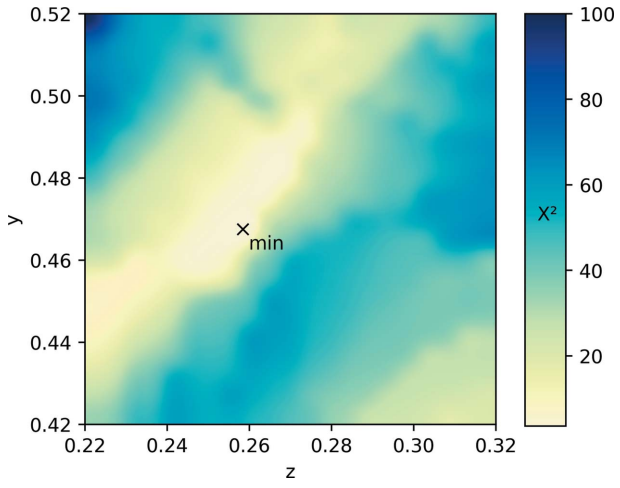


Figure 7
$X^2$ as a function of $z$ and $y$, parameters defining the oxygen positions.

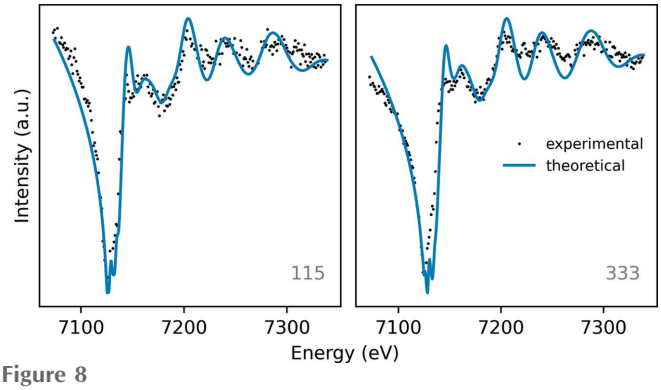


Figure 8
REXS spectra for the experimental 511 and 333 reflections compared with the theoretical data.

would improve the calculation statistics, leading to a more accurate determination. However, and in spite of the limited quantity of matter, we have been able to determine the oxygen-atom positions on a 25 nm thin film.

## 5. Conclusions

The position of the oxygen atoms, defined by the $x$ parameter in the bulk FVO sample, has been found to be the same for the Rietveld refinement of the S-XRD data – 0.262 (2) – and the approach we have presented in this study – 0.2627 (2) – which constitutes a proof of validation for our approach.

This method can be applied to thin-film systems, as we have shown for MgO//FVO. Despite the small quantity of matter, the oxygen positions have unambiguously been determined in a nondestructive way.

This approach follows the path of structural studies which use DANES to probe cations in thin films (Martin *et al.*, 2020) and pushes the method one step further, now probing indirectly the ligands which surround the cations. It can naturally be generalized to systems other than a spinel oxide. However, lower-symmetry systems may have more parameters to fit, requiring more simulation time and making the refinement process harder. When dealing with several parameters, instead of the complete meshing strategy, the $X^2$ minimization process might be done by an adequate choice of the simulation conditions, until the refinement process unequivocally converges into a single result.

To summarize, in this study we have proven the adequacy of a nondestructive REXS-based approach to determine the positions of oxygen atoms with a study performed on a bulk sample. We have then applied the method to a thin film to prove its efficiency in the case of a small amount of matter. The honing of this technique will enable the complete probing of the atomic positions in nanosized systems and will surely ease the conception of future thin-film-based devices.

## Acknowledgements

The authors thank the XRD and MEB-CRO platforms of the IPCMS. They are grateful to SOLEIL Synchrotron for providing access to the CRISTAL and DIFFABS beamlines and ESRF for access to the D2AM beamline. The authors declare that there is no conflict of interest.

## Funding information

This work of the Interdisciplinary Thematic Institute QMat, as part of the ITI 2021 2028 program of the University of Strasbourg, CNRS and Inserm, was supported by IdEx Unistra (ANR 10 IDEX 0002), and by SFRI STRAT'US project (ANR 20 SFRI 0012) and EUR QMAT ANR-17-EURE-0024 under the framework of the French Investments for the Future Program. The following funding is also acknowledged: Agence Nationale de la Recherche (award No. ANR-18-CECE24-0008-01).

## References

Alderman, O. L. G., Wilding, M. C., Tamalonis, A., Sendelbach, S., Heald, S. M., Benmore, C. J., Johnson, C. E., Johnson, J. A., Hah, H.-Y. & Weber, J. K. R. (2017). *Chem. Geol.* **453**, 169–185.
Bibes, M., Villegas, J. E. & Barthélémy, A. (2011). *Adv. Phys.* **60**, 5–84.
Blum, M.-M., Mustyakimov, M., Rüterjans, H., Kehe, K., Schoenborn, B. P., Langan, P. & Chen, J. C.-H. (2009). *Proc. Natl Acad. Sci. USA*, **106**, 713–718.
Bunău, O. & Joly, Y. (2009). *J. Phys. Condens. Matter*, **21**, 345501.
Eremin, M. V. (2019). *Phys. Rev. B*, **100**, 140404.
Favre-Nicolin, V. (1999). PhD thesis, Université Joseph-Fourier – Grenoble I, France.
Frank, P., Hodgson, K. O., Kustin, K. & Robinson, W. E. (1998). *J. Biol. Chem.* **273**, 24498–24503.
Frati, F., Hunault, M. O. J. Y. & de Groot, F. M. F. (2020). *Chem. Rev.* **120**, 4056–4110.
Giovannetti, G., Stroppa, A., Picozzi, S., Baldomir, D., Pardo, V., Blanco-Canosa, S., Rivadulla, F., Jodlauk, S., Niermann, D.,

Rohrkamp, J., Lorenz, T., Streltsov, S., Khomskii, D. I. & Hemberger, J. (2011). *Phys. Rev. B*, **83**, 060402.
Husain, H., Hariyanto, B., Sulthonul, M., Thamatkeng, P. & Pratapa, S. (2018). *IOP Conf. Ser. Mater. Sci. Eng.* **367**, 012027.
Joly, Y., Lorenzo, J. E., Nazarenko, E., Hodeau, J.-L., Mannix, D. & Marin, C. (2008). *Phys. Rev. B*, **78**, 134110.
Katcho, N. A., Richard, M. I., Landré, O., Tourbot, G., Proietti, M. G., Renevier, H., Favre-Nicolin, V., Daudin, B., Chen, G., Zhang, J. J. & Bauer, G. (2009). *J. Phys. Conf. Ser.* **190**, 012129.
Kawaguchi, S., Ishibashi, H., Nishihara, S., Mori, S., Campo, J., Porcher, F., Fabelo, O., Sugimoto, K., Kim, J., Kato, K., Takata, M., Nakao, H. & Kubota, Y. (2016). *Phys. Rev. B*, **93**, 024108.
Lefevre, C., Martin, E., Grenier, S., Roulland, F., Blanc, N., Boudet, N., Favre-Nicolin, V., Pourroy, G. & Viart, N. (2017). *XII e Colloque Rayons X et Matière. LILLIAD, LILLE, 14 au 17 Novembre 2017*, https://docplayer.fr/68271818-Xii-e-colloque-rayons-x-et-matiere-lilliad-lille-14-au-17-novembre-2017.html.
MacDougall, G. J., Garlea, V. O., Aczel, A. A., Zhou, H. D. & Nagler, S. E. (2012). *Phys. Rev. B*, **86**, 060414.
Maggay, I. V. B., De Juan, L. M. Z., Lu, J.-S., Nguyen, M. T., Yonezawa, T., Chan, T.-S. & Liu, W.-R. (2018). *Sci. Rep.* **8**, 8839.
Martin, E., Roulland, F., Grenier, S., Appert, F., Juraszek, J., Trassin, M., Bouillet, C., Chikoidze, E., Arnold, C., Berini, B., Dumont, Y., Colis, S., Barre, S., Versini, G., Preziosi, D., Leuvrey, C., Blanc, N., Boudet, N., Pourroy, G., Viart, N. & Lefèvre, C. (2020). *J. Alloys Compd.* **836**, 155425.
Nishihara, S., Doi, W., Ishibashi, H., Hosokoshi, Y., Ren, X.-M. & Mori, S. (2010). *J. Appl. Phys.* **107**, 09A504.
Rietveld, H. M. (1969). *J. Appl. Cryst.* **2**, 65–71.
Roisnel, T. & Rodríquez-Carvajal, J. (2001). *Mater. Sci. Forum*, **378–381**, 118–123.
Rotella, H., Copie, O., Steciuk, G., Ouerdane, H., Boullay, P., Roussel, P., Morales, M., David, A., Pautrat, A., Mercey, B., Lutterotti, L., Chateigner, D. & Prellier, W. (2015). *J. Phys. Condens. Matter*, **27**, 175001.
Roulland, F., Roseau, G., Corredor, A. P., Wendling, L., Krieger, G., Lefevre, C., Trassin, M., Pourroy, G. & Viart, N. (2022). *Mater. Chem. Phys.* **276**, 125360.
Shahzad, K., Khan, M. N., Shabbir, G. & Bashir, J. (2011). *Ferroelectrics*, **414**, 155–161.
Steciuk, G., David, A., Petříček, V., Palatinus, L., Mercey, B., Prellier, W., Pautrat, A. & Boullay, P. (2019). *J. Appl. Cryst.* **52**, 626–636.
Stragier, H., Cross, J. O., Rehr, J. J., Sorensen, L. B., Bouldin, C. E. & Woicik, J. C. (1992). *Phys. Rev. Lett.* **69**, 3064–3067.
Tan, G., Maruyama, K., Kanamitsu, Y., Nishioka, S., Ozaki, T., Umegaki, T., Hida, H. & Kanno, I. (2019). *Sci. Rep.* **9**, 7309.
Thomasson, A., Ibrahim, F., Lefevre, C., Autissier, E., Roulland, F., Mény, C., Leuvrey, C., Choi, S., Jo, W., Crégut, O., Versini, G., Barre, S., Alouani, M. & Viart, N. (2013). *RSC Adv.* **3**, 3124.
Trier, F., Noël, P., Kim, J.-V., Attané, J.-P., Vila, L. & Bibes, M. (2021). *arXiv*:2103.16271 [Cond-Mater].
Tröger, L., Arvanitis, D., Baberschke, K., Michaelis, H., Grimm, U. & Zschech, E. (1992). *Phys. Rev. B*, **46**, 3283–3289.
Vaz, D. C., Barthélémy, A. & Bibes, M. (2018). *Jpn. J. Appl. Phys.* **57**, 0902A4.
Woińska, M., Grabowsky, S., Dominiak, P. M., Woźniak, K. & Jayatilaka, D. (2016). *Sci. Adv.* **2**, e1600192.
Xie, W., Xing, X. & Cao, Z. (2019). *J. Appl. Phys.* **126**, 244904.
Zhang, Q., Singh, K., Guillou, F., Simon, C., Breard, Y., Caignaert, V. & Hardy, V. (2012). *Phys. Rev. B*, **85**, 054405.
Zhao, K.-H., Wang, Y.-H., Shi, X.-L., Liu, N. & Zhang, L.-W. (2015). *Chin. Phys. Lett.* **32**, 087503.
Zhou, Y., Zhang, Y. K., Yang, Q., Jiang, J., Fan, P., Liao, M. & Zhou, Y. C. (2019). *Comput. Mater. Sci.* **167**, 143–150.